

10. I. Daubechies, *Ten Lectures on Wavelets*, vol. 61 of *CBMS-NSF Regional Conference Series in Applied Mathematics*, SIAM Press, Philadelphia, 1992.
11. S. G. Mallat, "A theory for multiresolution signal decomposition: The wavelet decomposition," *IEEE Transactions on Pattern Analysis and Machine Intelligence* **11**, pp. 674–693, 1989.
12. A. Cohen, I. Daubechies, and J.-C. Feauveau, "Biorthogonal bases of compactly supported wavelets," *Communications on Pure and Applied Mathematics* **45**, pp. 485–500, 1992.
13. J. N. Bradley, C. M. Brislawn, and T. E. Hopper, "The FBI wavelet/scalar quantization standard for gray-scale fingerprint image compression," in *Visual Information Processing II*, F. O. Huck and R. D. Juday, eds., vol. 1961 of *SPIE Proceedings*, pp. x + 468, SPIE, SPIE, (Orlando, Florida), April 1993.
14. D. A. Huffman, "A method for the construction of minimum-redundancy codes," *Proceedings of the IRE* **40**, pp. 1098–1101, 1952.

Name	S/N	Name	S/N	Name	S/N
egys54u1/2	12.04/17.29	egys54s1/2	9.62/13.50	egys54a1/2	12.04/17.29
egys55u1/2	11.35/16.79	egys55s1/2	8.97/13.06	egys55a1/2	9.22/13.41
egys64u1/2	12.05/17.31	egys64s1/2	9.82/13.79	egys64a1/2	9.99/14.00
egys65u1/2	11.36/16.80	egys65s1/2	9.16/13.33	egys65a1/2	9.35/13.59
egym54u1/2	6.40/11.74	egym54s1/2	5.05/9.65	egym54a1/2	5.53/10.27
egym55u1/2	5.96/11.41	egym55s1/2	4.58/9.39	egym55a1/2	4.97/9.89
egym64u1/2	6.40/11.74	egym64s1/2	5.08/9.68	egym64a1/2	5.42/10.12
egym65u1/2	5.97/11.41	egym65s1/2	4.54/9.34	egym65a1/2	4.89/9.78
egyl54u1/2	12.69/16.50	egyl54s1/2	12.69/16.50	egyl54a1/2	12.64/16.21
egyl55u1/2	15.05/21.38	egyl55s1/2	12.16/16.17	egyl55a1/2	12.09/15.89
egyl64u1/2	15.59/21.91	egyl64s1/2	12.67/16.50	egyl64a1/2	12.56/16.21
egyl65u1/2	15.05/21.40	egyl65s1/2	12.13/16.16	egyl65a1/2	12.05/15.91
tris54u1/2	33.05/33.72	tris54s1/2	29.18/29.34	tris54a1/2	23.12/22.82
tris55u1/2	33.05/33.72	tris55s1/2	28.41/28.64	tris55a1/2	22.84/22.61
tris64u1/2	33.06/33.74	tris64s1/2	29.22/29.36	tris64a1/2	23.85/23.49
tris65u1/2	32.55/33.34	tris65s1/2	28.43/28.65	tris65a1/2	23.42/23.16
trim54u1/2	26.40/27.54	trim54s1/2	23.64/24.38	trim54a1/2	18.36/18.67
trim55u1/2	25.63/26.87	trim55s1/2	23.01/23.84	trim55a1/2	17.73/18.14
trim64u1/2	26.31/27.46	trim64s1/2	23.62/24.38	trim64a1/2	18.40/18.78
trim65u1/2	25.58/26.80	trim65s1/2	23.09/23.94	trim65a1/2	17.80/18.30
tril54u1/2	36.70/37.82	tril54s1/2	28.15/27.11	tril54a1/2	26.34/26.08
tril55u1/2	36.15/37.32	tril55s1/2	27.67/26.68	tril55a1/2	25.94/25.74
tril64u1/2	36.70/37.83	tril64s1/2	28.22/27.14	tril64a1/2	26.60/26.49
tril65u1/2	36.15/37.33	tril65s1/2	27.82/26.77	tril65a1/2	26.25/26.20

Table 1. Signal-to-noise ratios for various parameter choices, at 25:1 compression.

REFERENCES

1. R. R. Coifman, Y. Meyer, S. R. Quake, and M. V. Wickerhauser, "Signal processing and compression with wavelet packets," in *Progress in Wavelet Analysis and Applications*, Y. Meyer and S. Roques, eds., Proceedings of the International Conference "Wavelets and Applications," Toulouse, France, 8–13 June 1992, pp. 77–93, Editions Frontieres, Gif-sur-Yvette, France, 1993.
2. R. Devore, B. rn Jawerth, and B. J. Lucier, "Image compression through wavelet transform coding," *IEEE Transactions on Information Theory* **38**, pp. 719–746, March 1992.
3. J. Lu, V. R. Algazi, and J. Robert B. Estes, "Comparative study of wavelet image coders," *Optical Engineering* **35**, pp. 2605–2619, September 1996.
4. P. Mathieu, M. Barlaud, and M. Antonini, "Compression d'images par transformée en ondelette et quantification vectorielle," *Traitement du Signal* **7**(2), pp. 101–115, 1990.
5. O. Rioul, "On the choice of wavelet filters for still image compression," in *Proceedings of ICASSP'93*, vol. V, pp. 550–553, IEEE Press, 1993.
6. M. V. Wickerhauser, "Comparison of picture compression methods: Wavelet, wavelet packet, and local cosine transform coding," in *Wavelets: Theory, Algorithms, and Applications*, C. K. Chui, L. Montefusco, and L. Puccio, eds., Proceedings of the International Conference in Taormina, Sicily, 14–20 October 1993, pp. 585–621, Academic Press, San Diego, California, 1994.
7. P. L. Donoho, R. A. Ergas, and J. D. Villasenor, "High-performance seismic trace compression," in *Proceedings of SEG*, pp. 160–163, 1995.
8. E. Reiter and M. Hall, "A comparison of multi-dimensional wavelet compression methods," in *Proceedings of EAGE*, 1996.
9. M. V. Wickerhauser, *Adapted Wavelet Analysis from Theory to Software*, AK Peters, Ltd., Wellesley, Massachusetts, 1994.

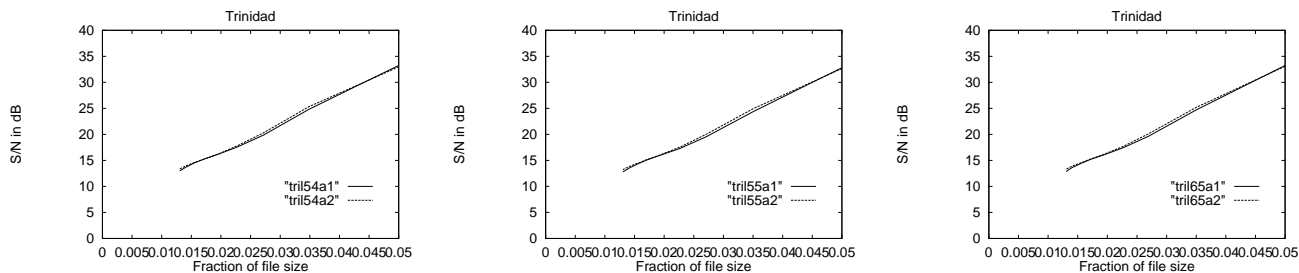


Figure 7. 5/4, 5/5, and 6/5 level decompositions applied to long filters and adjusted quantizations for the Trinidad survey data.

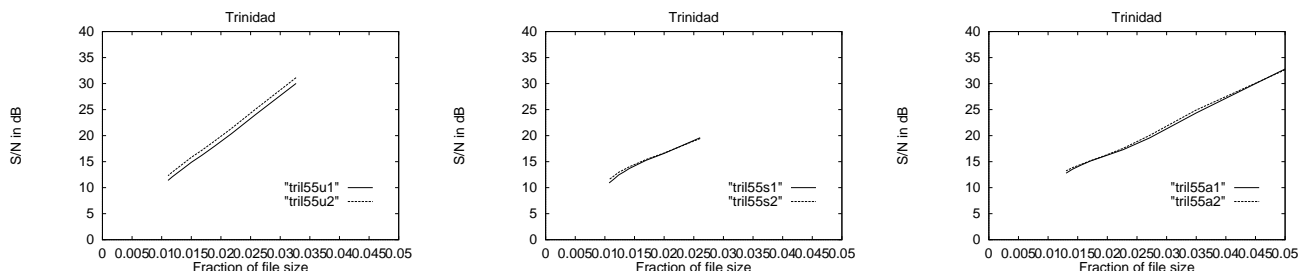


Figure 8. Uniform, subbanded, and adjusted quantization applied to long filters to 5/5 levels for the Trinidad survey data.

4. Comparisons

In this study we did not consider other wavelet representations, such as local cosines, best orthogonal bases, or multiwavelets. In addition, we did not look at different encoding schemes. These two topics will be the subject of a future paper.

We chose an arbitrary compression ratio (25:1) and estimated the signal to noise ratio after compression by the 36 various methods and the two measures of distortion. This was done by fitting the least-squares line through the pairs (file fraction, S/N) for each parameter choice, then evaluating that linear function at the file fraction 0.040. The results are given in Table 1 below.

It should be noted that the two distortion criteria used here are not perfectly correlated with visible distortion. Thus, an individual subject may prefer one of the lower signal-to-noise reconstructions, obtained through visibility-adjusted quantization. Another measure of quality might be the statistics of the residual, which ideally should be white noise. The residual produced by subband-variance-weighted or adjusted quantization, though more energetic, in some cases has fewer visible features of the original signal. It is difficult to reconcile these conflicting notions of quality without precise knowledge of the ultimate “customer” for the data, be he man or machine. Our goal therefore is to be *unbiased*, that is, to make the fewest assumptions about the customer’s vision and intended use for the data.

5. Conclusion

This study showed results of different 2-D wavelet image coders on two seismic data sets. We used a comprehensive representation of filter lengths, decomposition levels, quantization schemes, and compression ratios. The results show that, for both data sets used, we get the least average error at a given compression by using long filter lengths, moderate decomposition levels and variance weighted subband quantization scheme adjusted with a subband visibility matrix. More specifically, the best combination seems to be the (9, 7) biorthogonal filter decomposition to levels (6, 4) in time and trace number, coupled with uniform quantization. These parameter choices are very significant for the design of efficient 3-D wavelet image coders for fast compression of 3-D seismic data. This study is by no means exhaustive; future studies are envisioned to evaluate compression using local cosines, best orthogonal bases, multiwavelets, and different encoding schemes.

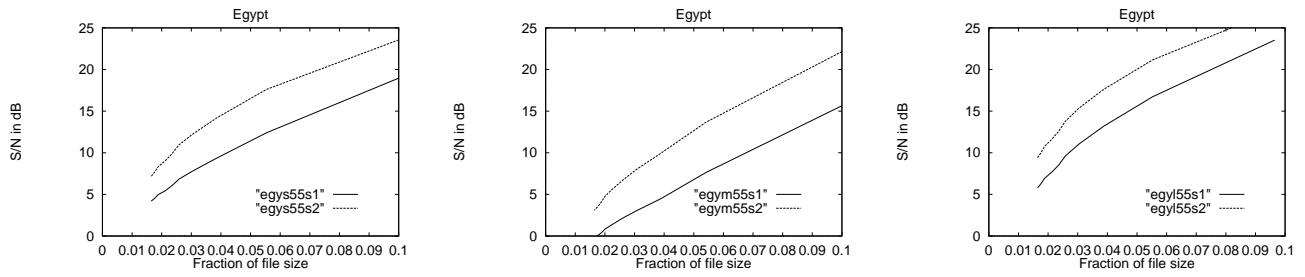


Figure 3. Short, medium, and long filters applied to 5/5 level decompositions and subbanded quantization for the Egypt survey data.

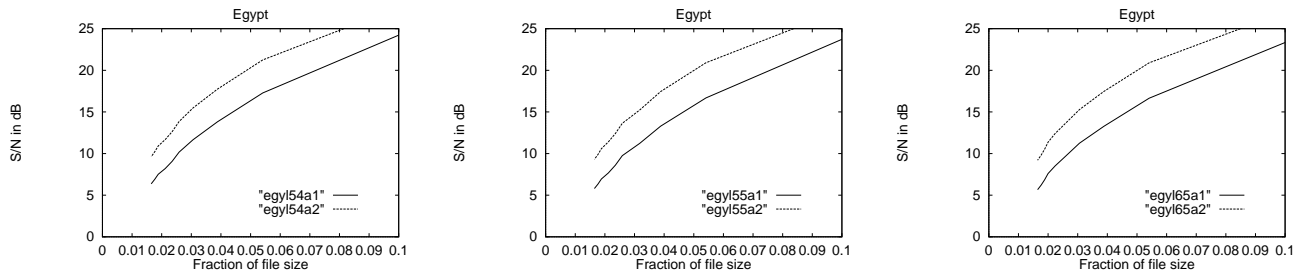


Figure 4. 5/4, 5/5, and 6/5 level decompositions applied to long filters and adjusted quantizations for the Egypt survey data.

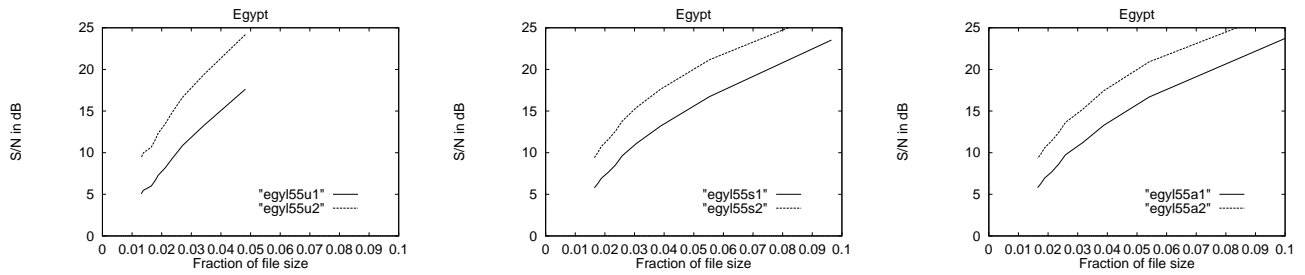


Figure 5. Uniform, subbanded, and adjusted quantization applied to long filters to 5/5 levels for the Egypt survey data.

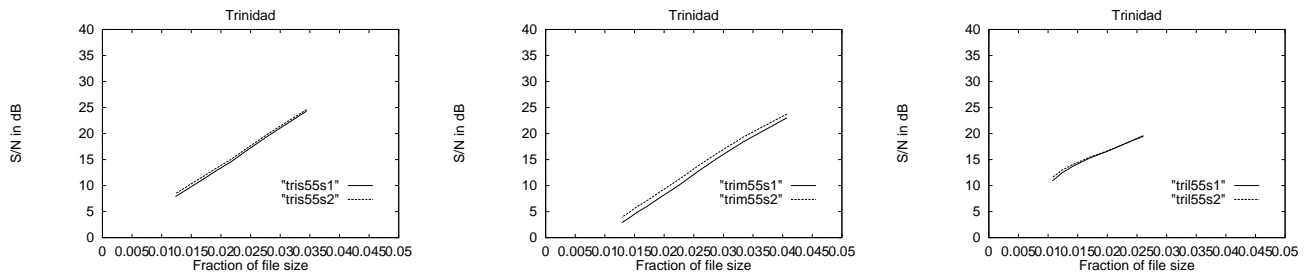


Figure 6. Short, medium, and long filters applied to 5/5 level decompositions and subbanded quantization for the Trinidad survey data.

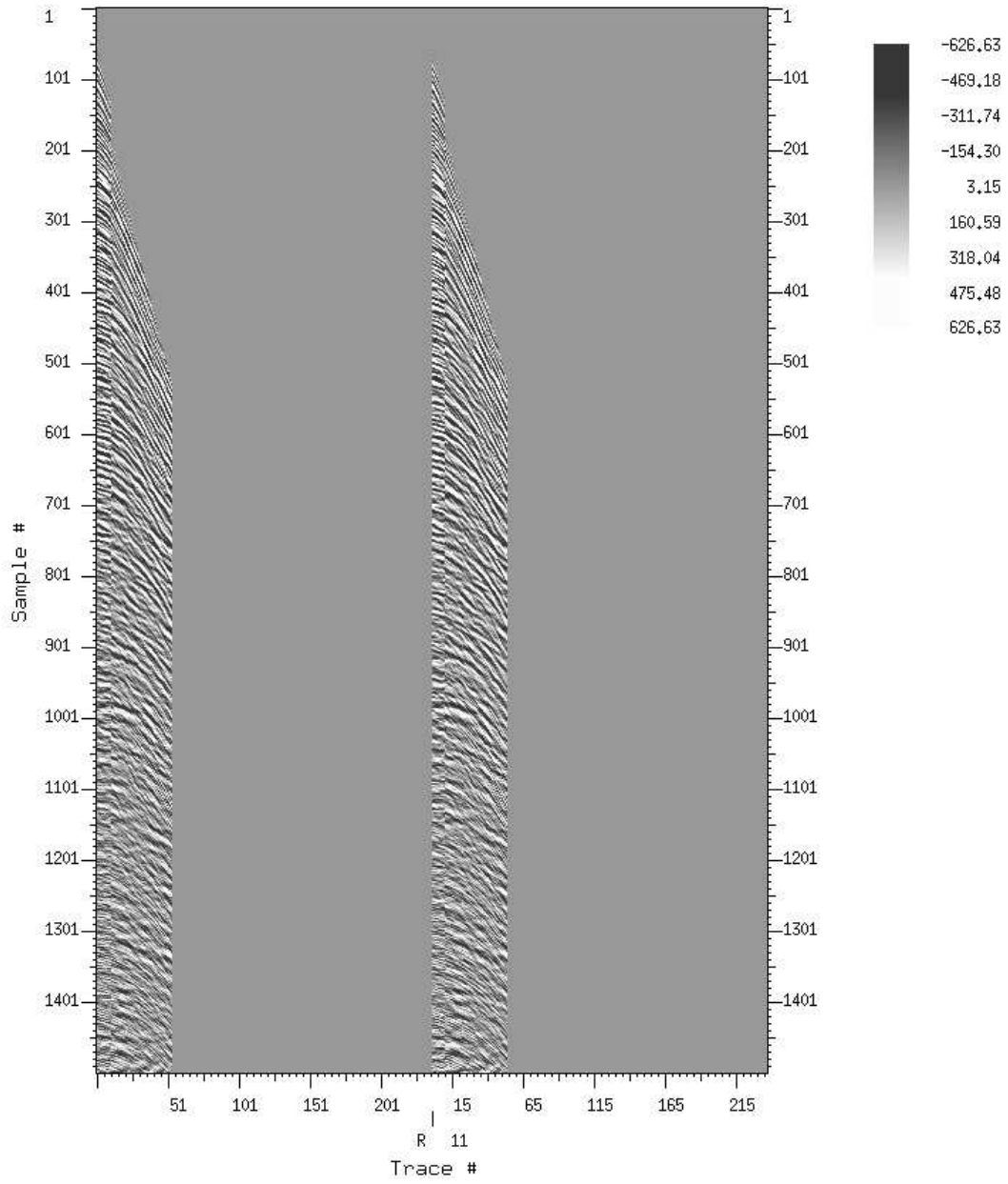


Figure 2. Density plot of several traces from the Trinidad survey.

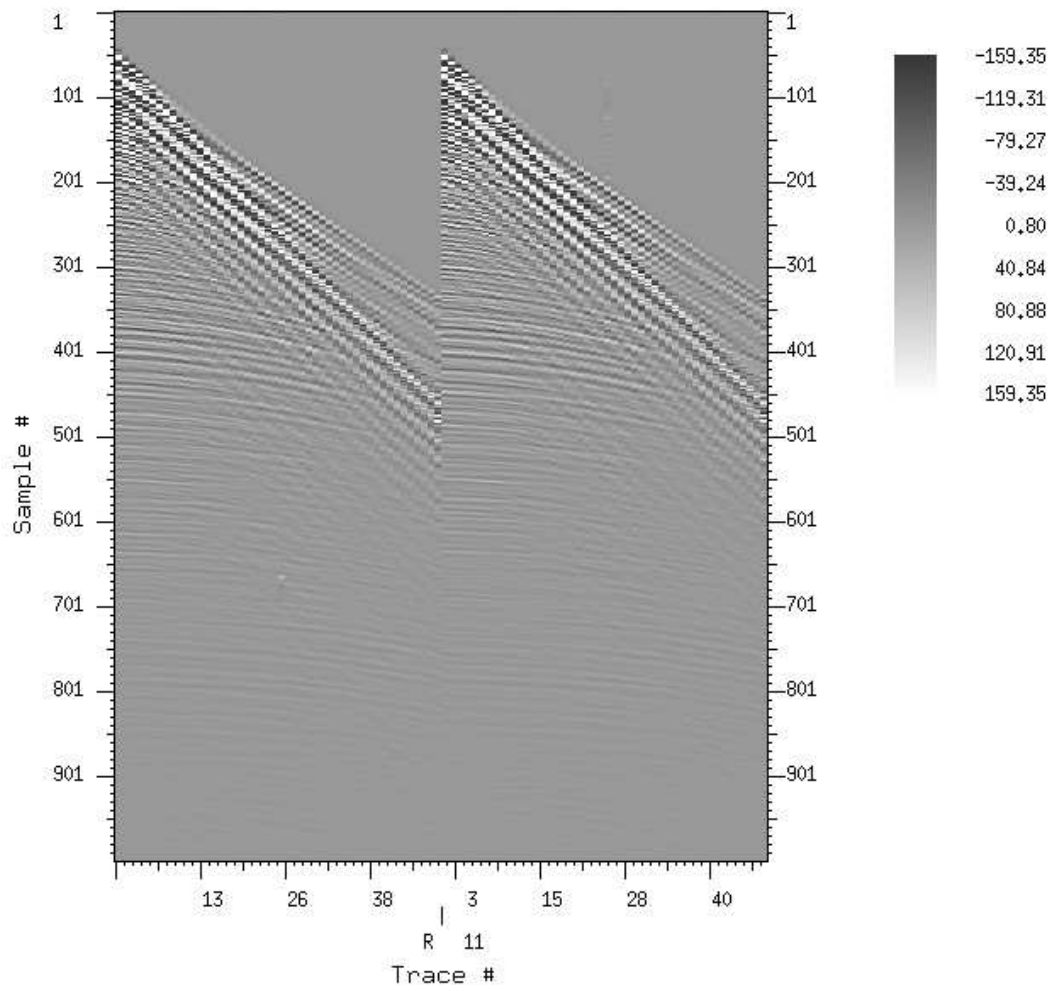


Figure 1. Density plot of several traces from the Egypt survey.

several other choices of visual adjustment array. As to the subband variance, subbands with small variance as for instance high frequency subbands, are assigned coarse bin widths. In contrast, low frequency subbands are assigned fine bin widths. In this study, the non-zero bin width is inversely proportional to the logarithm of the subband variance.

The zero bin width at each subband is assigned 1.2 times the value of the non-zero bin width and the reconstructed value from each subband non-zero quantization bin corresponds to a value slightly smaller than the bin midpoint value. In our study we have all three scalar quantization techniques described above, namely scalar uniform quantization, variance-weighted quantization and variance weighted quantization with a sub-band visual adjustment array.

2.3. Lossless Encoding Techniques

In this step, we attempt to map the set of quantized coefficients to a set of symbols, so that the total number of bits per symbol gets minimized. The encoding process works with the the probabilities of the quantized coefficients. If these coefficients are stationary, then Huffman coding¹⁴ plus zero-run-length coding can be efficiently used. However, if these coefficients are not stationary, then more sophisticated coding such as arithmetic coding have to be used. In this study we used Huffman coding plus zero-run-length coding.

3. Experiment Parameters

We designed this compression comparison experiment so that it accomodates some seismic data variety and a good selection of compression parameters. In terms of seismic data, we worked with two data sets, all of them two-dimensional slices from three-dimensional offshore surveys, one from Egypt and one from Trinidad. These two data sets are displayed in Figures 1 and 2, respectively. Which data set was used may be determined from the first three letters of the plot label. Egyptian data is named `egy*****`, while Trinidad data is named `tri*****`.

In terms of compression parameters, we used three previously described filters.¹² All three filters are biorthogonal and come in quadruplets, with an analysis pair and its conjugate synthesis pair. The short, medium and long analysis filter pairs have (5, 3), (8, 4), and (9, 7) taps, respectively. In fact the longest filter is the same used by the FBI for fingerprint compression. Which filter set was used can be determined from the fourth letter in the plot label; `****s****` stands for short or (5, 3), `****m****` stands for medium or (8, 4), and `****l****` stands for long or (9, 7).

We used four different levels of decomposition: (5, 4), (5, 5), (6, 4), and (6, 5), with the first number representing the time decomposition and the second representing the trace decomposition. Which levels were used can be determined from the two-digit number in positions five and six of the plot label; `****54**` stands for (5, 4), and so on.

Finally, we employed three different quantization schemes. The first scheme computes a uniform zero and non-zero coefficient bin, while the other two perform variance weighted subband quantization. The different between these last two quantization schemes is that the first assumes a flat subband visibility model, while the second quantization scheme allows for an adjusted visual model which increases the bin widths for the high resolution subbands. Which of these was used can be deduced from the seventh character in the plot label: `*****u*` stands for **u**niform quantization, `*****s*` stands for a flat subband model, while `*****a*` stands for an **a**adjusted visual model.

Therefore, for each data set we have three different filter choices, four different decomposition levels and three different quantization schemes, resulting in 36 different data compressed and decompressed files. For each of the 36 resulting compressed and decompressed files we compute two signal-to-noise ratios (S/N, in dB) using the following formulas:

$$(1) \quad \text{Abs. S/N} = 20 \log_{10} \left(\frac{\sum_k |c_k|}{\sum_k |\Delta c_k|} \right); \quad (2) \quad \text{MSE S/N} = 10 \log_{10} \frac{\sum_k |c_k|^2}{\sum_k |\Delta c_k|^2}.$$

Which formula was used to find distortion may be determined from the last digit in the plot label: `*****1` stands for formula (1), while `*****2` stands for formula (2).

We then plot these S/N ratios *versus* the fractional file size. These plots are then compared for each of the three original data sets and the parameters leading to the best compression results are flagged. Several of the 72 plots are shown in Figures 3 through 8, for comparison.

2. Wavelet Image Coding

It is well known that wavelet image coding consists of three main parts: wavelet transform, quantization, and redundancy removal. This section is mostly a review of wavelet image coding schemes and in particular of the parameter choices used in wavelet transform and quantization. In this study we have not looked at different encoding schemes like arithmetic coding. This is an issue which should be further investigated in the near future. The subject of wavelet transform coding has been well referenced in a lot of journal articles, thus in this review section, we refer the interested reader to other papers and texts.⁹

2.1. Wavelet transform schemes

In this study we work only with 2-D separable wavelet transform, which means that we only have to concern ourselves with their corresponding 1-D wavelets and scaling functions. There are two families of wavelets, orthogonal and biorthogonal. Orthogonal wavelets have several interesting properties. First, they provide an orthonormal basis system for square integrable functions, *i.e.*, finite-energy signals. Second, they can have compact support, or in filtering terms they can have a finite impulse response, thus allowing for very efficient computer implementation. Third, we need only one FIR filter function to be defined, and that is the scaling function, the mother wavelet is determined from the scaling function through a quadrature mirror filter relation.¹⁰ Another study⁵ has indicated that optimum image compression for still images is obtained with filter lengths ranging between 8 and 10. However, the compactly supported wavelets have asymmetric finite impulse response. As a result, their phase is non-linear which in turn can cause artifacts in the decompressed images. One way to avoid this problem in orthogonal filters is to use orthogonal wavelets which are not compactly supported. Realistically, since we want to work with FIR filters we have to work with a long subset of the noncompactly supported wavelet coefficients, which are fast decaying, at the expense of more CPU time. This is not the preferred way to achieve computationally efficient compression. The other wavelet choice, biorthogonal wavelets, are both compactly supported and have symmetric impulse response. Besides symmetry, another major difference between orthogonal and biorthogonal wavelets is biorthogonal wavelets use one pair of functions for the forward wavelet transform and one pair of filters for the inverse transform. The pair of the forward transform filters are not orthogonal to each other, but they are orthogonal to the pair of the inverse wavelet transform filters. The computational cost incurred by using biorthogonal wavelets instead of orthogonal wavelets is small, with the added advantage of a linear phase filter response. For both orthogonal and biorthogonal wavelets there are fast computational algorithms,¹¹ which allow very efficient wavelet transform computation.

In this study we have used biorthogonal filters with different filter lengths. We used three different filters, short, medium and long. The short, medium and long filters had (5, 3), (8, 4), and (9, 7) filter lengths for both the forward and the inverse transform.¹² The long filter is the same one used by FBI for fingerprint compression and decompression and identification.¹³ We also used different combinations for wavelet transform decomposition levels. In particular we used four combinations for the wavelet decomposition in time and space: 5/4, 5/5, 6/4 and 6/5. Each of these decomposition level pairs was combined with the three different filters in a search for the optimum compression scheme.

2.2. Quantization Schemes

The result of applying the wavelet transform is a set of coefficients of which most have very small amplitudes and only few have significant values. In order to get compression, we map the set of wavelet transform coefficients to a new set of discrete values. This process of mapping from a continuous set of real values to a set of discrete values is called quantization.

In general there are two kinds of quantization, first scalar quantization and second vector quantization. In scalar quantization, each wavelet coefficient or sample in general is quantized. In vector quantization several samples are quantized together and in general, vector quantization is more powerful than scalar quantization. In this paper we work with scalar quantization. There are several sub-types of scalar quantization. The first type is uniform scalar quantization. In this quantization, we assign two bin widths for all samples, or in this case wavelet coefficients, one for the significant sample values and one for the close to zero values. The second type is scalar quantization, with different quantization bins per subband. The non-zero bin width per subband is determined by two factors, first an adjustable subband array related to human vision, and second the subband coefficient variance. The adjustable array can be user defined. The easiest choice is to have a unit array across all subbands. In this study we have looked at

Comparison of Wavelet Image Coding Schemes for Seismic Data Compression*

Anthony Vassiliou^a and Mladen Victor Wickerhauser^b

^aAmoco EPTG, 4502 E. 41 St., Tulsa, OK 74135

^bDept. of Math., Washington University, St. Louis, MO 63130

ABSTRACT

Wavelet transform coding image compression is applied to two raw seismic data sets. The parameters of filter length, depth of decomposition, and quantization method are varied through 36 parameter settings and the rate-distortion relation is plotted and fitted with a line. The lines are compared to judge which parameter setting produces the highest quality for a given compression ratio on the sample data. It is found that long filters, moderate decomposition depths, and frequency-weighted, variance-adjusted quantization yield the best results.

1. Introduction

Wavelet image compression has been a very active research subject during the last few years.¹⁻⁶ However, application of wavelet image coding to seismic data compression has only started very recently.^{7,8} Seismic data compression presents more difficulties than still image compression, due to certain image discontinuities (such as residual statics) and large image amplitude imbalances. Nevertheless, seismic data compression has been applied with good success in several case studies, achieving compression ratios of 10:1 to 50:1 for 2-D seismic data and 30:1 to 150:1 for 3-D seismic data. Since the subject of seismic data compression is fairly new, there has not been up to now any comprehensive comparative study of wavelet image coding for 2-D seismic data compression. The unavailability of such study makes it very hard to design efficient wavelet image coders for 3-D seismic data compression, where there are significant many more choices of wavelet coding options. Due to these reasons, we studied several wavelet image coders and their behavior in 2-D seismic data compression.

Since there are many forms that seismic data can be available, for instance raw shot gather data, common-offset data, etc., in this study we are working with only one particular form of seismic data. This form, is called common depth point gathers (CDP), and is obtained from sorting in almost real time, raw shot gather data, according to their common depth or reflection point. Assuming that there are no significant image discontinuities in the data, such as residual statics, efficiently compressed CDP seismic data can then be transmitted via satellite during large offshore seismic 3-D surveys to the processing center. In the processing center the data are decompressed, quality checked and then processed through a typical seismic data processing flow. We have collected a set of about 100 CDP gathers, from four different areas of the world which have been compressed with several wavelet image coders. In this preliminary study, we use several of these from two of the areas.

The class of compression algorithms which are explored in this project, use the separable discrete wavelet transform (DWT) which is then followed by uniform, weighted, or frequency-adjusted quantization and zero-run-length plus static Huffman coding. We examine the effectiveness of these algorithms for different choices of parameters for wavelet transform coding and quantization. For each of these parameter choices and for each data set we compress the data set using several compression ratios from 5:1 up to 100:1 and then we compute the actual bit rate achieved as well as the distortion in terms of the residual energy. We then present the composite results of bit rate *versus* distortion for each parameter choice. The parameters which yield lower distortion bit rate at a given bit rate are the best choices.

This paper is organized as follows. Section II, reviews wavelet transform image coding by looking at several choices of wavelets and quantization schemes. In section III we describe the distortion measures employed in this study. In section IV we present the results of the seismic data compression and we conclude this study with section V.

*Research supported by NSF, AFOSR, Amoco Inc., and the Southwestern Bell Telephone Company